Monthly Notices
of the
ROYAL ASTRONOMICAL SOCIETY

MNRAS **477,** L70–L74 (2018)
Advance Access publication 2018 March 14

doi:10.1093/mnrasl/sly043

Discovery of three strongly lensed quasars in the Sloan Digital Sky Survey

P. R. Williams,[1⋆] A. Agnello,[2⋆] T. Treu,[1] L. E. Abramson,[1] T. Anguita,[3,4] Y. Apostolovski,[3,4] G. C.-F. Chen,[5] C. D. Fassnacht,[5] J.-W. Hsueh,[5] B. C. Lemaux,[5] V. Motta,[6] L. Oldham,[7] K. Rojas,[6] C. E. Rusu,[5] A. J. Shajib[1] and X. Wang[1]

[1]*Department of Physics and Astronomy, PAB, 430 Portola Plaza, Box 951547, Los Angeles, CA 90095-1547, USA*
[2]*European Southern Observatory, Karl-Schwarzschild-Strasse 2, D-85748 Garching bei München, Germany*
[3]*Departamento de Ciencias Físicas, Universidad Andres Bello, Fernandez Concha 700, Las Condes, 7591538, Santiago, Chile*
[4]*Millennium Institute of Astrophysics (MAS), Nuncio Monseñor Sótero Sanz 100, Providencia, 9500011, Santiago, Chile*
[5]*Department of Physics, University of California, Davis, 1 Shields Avenue, Davis, CA 95616, USA*
[6]*Instituto de Física y Astronomía, Universidad de Valparaíso, Avda. Gran Bretaña 1111, Playa Ancha, Valparaíso 2360102, Chile*
[7]*Institute of Astronomy, University of Cambridge, Madingley Road, Cambridge CB3 0HA, UK*

Accepted 2018 March 9. Received 2018 March 5; in original form 2017 June 5

ABSTRACT

We present the discovery of three quasar lenses in the Sloan Digital Sky Survey, selected using two novel photometry-based selection techniques. The J0941+0518 system, with two point sources separated by 5.46 arcsec on either side of a galaxy, has source and lens redshifts 1.54 and 0.343. Images of J2257+2349 show two point sources separated by 1.67 arcsec on either side of an E/S0 galaxy. The extracted spectra show two images of the same quasar at $z_s = 2.10$. SDSS J1640+1045 has two quasar spectra at $z_s = 1.70$ and fits to the SDSS and Pan-STARRS images confirm the presence of a galaxy between the two point sources. We observed 56 photometrically selected lens candidates in this follow-up campaign, confirming three new lenses, re-discovering one known lens, and ruling out 36 candidates, with 16 still inconclusive. This initial campaign demonstrates the power of purely photometric selection techniques in finding lensed quasars.

Key words: gravitational lensing: strong – methods: observational.

1 INTRODUCTION

Strong gravitational lensing serves as a unique probe into the distant universe (e.g. Treu & Ellis 2015, and references therein). One can use lenses as cosmic telescopes to study, e.g. the properties of quasar hosts at high redshifts (Peng et al. 2006; Ding et al. 2017). Anomalies in image positions and fluxes can be used to probe dark matter substructure in the lensing object (Mao & Schneider 1998; Dalal & Kochanek 2002; Vegetti et al. 2012; Nierenberg et al. 2014). Microlensing due to compact objects in the lens galaxy (see Wambsganss 2006) can be used to study the inner structure of lensed active galactic nuclei (AGNs), enabling measurements of the accretion disc size (Kochanek 2004; Motta et al. 2017) and thermal slopes (Anguita et al. 2008; Eigenbrod et al. 2008) and the geometry of the broad line region (Braibant et al. 2014, 2016). With additional monitoring, one can use the delay between arrival of the images as a cosmological distance indicator (e.g. Refsdal 1964; Schechter et al. 1997; Tewes, Courbin & Meylan 2013; Suyu et al. 2014; Bonvin et al. 2016; Treu & Marshall 2016).

Unfortunately, this field of research is limited by the small number of known lenses. Since strong gravitational lensing requires such a close alignment of a distant source with a foreground lensing object, lensed quasars are rare objects. Oguri & Marshall (2010) estimate that, given an *i*-band limiting magnitude of 21, there are ∼0.2 lenses per square degree, of which ≈20 per cent are information-rich quads. Thus, the large footprints of wide-field surveys [e.g. the Sloan Digital Sky Survey (SDSS, York et al. 2000), Dark Energy Survey (DES, Diehl et al. 2014), Kilo-Degree Survey (de Jong et al. 2013), Panoramic Survey Telescope and Rapid Response System (Pan-STARRS, Chambers et al. 2016)] are essential for successful searches.

Previous systematic searches for strongly lensed quasars have predominantly explored samples of objects with spectroscopic data. The Cosmic Lens All Sky Survey (Browne et al. 2003; Myers et al. 2003) with the Jodrell-Bank VLA Astrometric Survey (King et al. 1999) explored flat-spectrum radio sources, resulting in the discovery of 22 lenses. In the optical, Pindor et al. (2003) compared single- and double-component fits to spectroscopically confirmed quasars in SDSS to identify closely separated pairs as lens candidates. The SDSS Quasar Lens Search (Oguri et al. 2006; Inada et al. 2012) explored low-redshift ($0.6 < z < 2.2$) spectroscopically confirmed

⋆ E-mail: pwilliams@astro.ucla.edu; aagnello@eso.org

quasars, using a morphological selection to find small-separation candidates and a colour-based selection to find lenses that are deblended in SDSS imaging. More recently, More et al. (2016) applied a similar method to the Baryon Oscillation Spectroscopic Survey (Dawson et al. 2013), expanding the SDSS spectroscopic searches out to higher redshifts.

To expand searches to include the footprints of new and upcoming wide-field surveys, photometry-based techniques have been developed. Ostrovski et al. (2017) use Gaussian Mixture Models to search the DES Y1A1 (Diehl et al. 2014) footprint using DES photometry with the Wide-field Infrared Survey Explorer (Wright et al. 2010) and VISTA Hemisphere Survey (McMahon et al. 2013) infrared bands. Agnello et al. (2015) used an artificial neural network classifier applied to blue, extended objects, and Lin et al. (2017) search for red galaxies with multiple blue neighbours in DES.

In this paper, we present the discovery of three new strongly lensed quasars selected by two independent photometry-based techniques applied to the SDSS DR12 footprint: J0941+0518 at (RA, Dec.) = (09:41:22.5, +05:18:23.9), J1640+1045 at (16:40:18.2, +10:45:05.1), and J2257+2349 at (22:57:25.4, +23:49:30.4). The quasar images are separated by 5.46, 2.20, and 1.67 arcsec, and correspond to sources at $z_s = 1.54$, 1.70, and 2.11, respectively. We also present the blind re-discovery of the lens HS 2209+1914 at (RA, Dec.) = (22:11:30.3, +19:29:13.2) and provide AO-assisted images showing the presence of an Einstein ring. In Section 2, we describe the follow-up of lens candidates, and in Section 3, we provide model fits to the three newly discovered lenses. Finally, we conclude in Section 4.

2 CANDIDATE SELECTION AND FOLLOW-UP

Candidates were selected using two photometry-based methods described in Williams, Agnello & Treu (PopMix, 2017) and Agnello (OutlierSel, 2017), applied to SDSS-DR12 data. The methods produced lists of 59 and ∼250 candidates, respectively, from which 21 and 36 were selected for imaging and spectroscopic follow-up. A complete discussion of candidate sample size with choice of cuts is given in the respective paper.

Candidates were observed using the Near-Infrared Camera 2 (NIRC2), the Echellette Spectrograph and Imager (ESI, Sheinis et al. 2002), the OH-Suppressing InfraRed Imaging Spectrograph (OSIRIS, Larkin et al. 2006), and the DEep Imaging Multi-Object Spectrograph (DEIMOS, Faber et al. 2003) at Keck Observatory; the ESO Faint Object Spectrograph and Camera (EFOSC2, Buzzoni et al. 1984) at the New Technology Telescope; and the Adaptive Optics Module and Goodman Spectrograph at the Southern Astrophysical Research Telescope. In this campaign, we observed 56 total candidates (Table 1), including three new lenses and one known lens, described below.

2.1 SDSS J0941+0518

SDSS J0941+0518 was identified both by the PopMix and OutlierSel methods. Additionally, the galaxy and one quasar image have spectra in SDSS which identify the sources as a galaxy and quasar, respectively. The galaxy spectrum is blended with the second quasar image spectrum and shows a C IV feature at the expected wavelength based on the other quasar image's redshift.[1]

Images were obtained with the OSIRIS Imager on 2016 November 9 (Kbb filter, $\lambda_{cent} = 2172$ nm, bandwith 415 nm, plate scale 0.02 arcsec per pixel, 27 exposures of 30 s, 3 arcsec dithers). Spectra were obtained with ESI on 2016 November 19 (echellette mode, 0.75 arcsec slit, wavelength coverage 3900–10900 Å, three 600 s exposures with dithers).

Images show two point sources separated by 5.4554 ± 0.0003 arcsec on either side of the lens galaxy (Fig. 1). The spectra (Fig. 2) are consistent with coming from the same object at $z_s = 1.54$, based on the C III] and Mg II lines. The galaxy spectrum with the Ca H and K, *G*-band, Mg b, and Na D lines gives $z_l = 0.343$. These values agree with the SDSS spectra which give $z_s = 1.55$ and $z_l = 0.343$.

2.2 SDSS J2257+2349

SDSS J2257+2349 was identified by the OutlierSel method. AO-assisted images were obtained with NIRC2 on 2016 September 21 (narrow camera, Kp filter, $\lambda_{cent} = 2124$ nm, bandpass 351 nm, plate scale 0.01 arcsec per pixel). Two sets of three 120 s exposures were taken using a three-point dither pattern in addition to two 60 s acquisition exposures. Spectra were obtained with EFOSC2 on 2016 September 27 (Gr#13 grism, 1.2 arcsec slit, wavelength coverage 3685–9315 Å, dispersion 5.54 Å per pixel).

Images show two point sources separated by 1.6701 ± 0.0036 arcsec on either side of an E/S0 galaxy (Fig. 1). The point sources correspond to the same quasar at $z_s = 2.11$, based on the Si IV + O IV], C IV, and C III] lines.

2.3 SDSS J1640+1045

SDSS J1640+1045 was identified by the OutlierSel method and *Gaia* multiplet detection (Agnello 2017).[2] Spectra were obtained with DEIMOS on 2017 March 29 (1.0 arcsec slit, 600ZD grating, $\lambda_{cent} = 7150$ Å, GG455 order-blocking filter, 360 s exposure time). The results show two quasar spectra at $z_s = 1.70$, based on the C III], C II], Mg II, and [Ne V] lines.

This object has not been followed up with AO-assisted imaging, so we obtained positions and fluxes by modelling seeing-limited images from Pan-STARRS and SDSS. Models consist of two point sources and a galaxy. The quasar images (resp. galaxy) dominate in bluer (resp. redder) bands, and the structural parameters of the lens are systematically affected by proximity with the brightest quasar image (appreciably across different bands). Thus, we choose a de Vaucouleurs profile for the surface brightness of the lens, perform the fit in separate bands, and list the weighted averages of positions and effective radius.

The model converges for the four reddest bands in each set of images, but fails to converge for the bluest images. We show the model fits and residuals for the Pan-STARRS image cutouts in Fig. 3. Combining the fits for all SDSS and Pan-STARRS bands and setting the brighter Image A at the origin, we find the component positions to be $(x, y) = (0.00 \pm 0.01, 0.00 \pm 0.02)$ arcsec (Image A), $(1.80 \pm 0.01, 1.36 \pm 0.06)$ arcsec (Image B), and $(0.43 \pm 0.04,$

[1] After this paper was submitted, we learned that Claude Cornen had independently found this lens and posted it on Galaxy Zoo, https://talk.galaxyzoo.org/#/boards/BHZ0000001/discussions/DGZ000167u?page=3

[2] This system was also confirmed, in mid-April 2017, by an independent search (C. Lemon, private communication and in preparation).

Table 1. List of all observed candidates along with their selection method, observing outcome, and lens and source redshift, if available. The full table with all 56 candidates is available online.

Name	RA (J2000)	Dec. (J2000)	mag_i	Selection method	Instrument	Comments	z_s	z_l
J0941+0518	145.343 5481	5.306 9880	21.39, 17.44, 18.51	PopMix, OutlierSel	ESI, OSIRIS		1.54	0.343
J1640+1045	250.075 9898	10.751 4136	17.84	OutlierSel	DEIMOS		1.70	
J2257+2349	344.355 8623	23.825 1034	17.67	OutlierSel	EFOSC2, NIRC2		2.11	
J2211+1929	332.876 3774	19.486 9926	15.41	PopMix	EFOSC2, ESI, NIRC2	HS 2209+1914	1.07	
J0048+2505	12.145 7148	25.089 6541	18.77	OutlierSel	NIRC2	Two point sources		

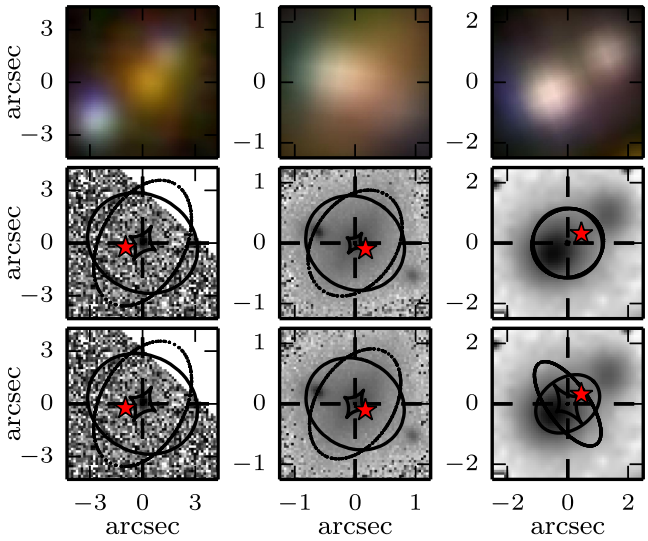

Figure 1. *Top to bottom:* SDSS postage stamps, SIE model fits, and SIE+fluxes model fits to the newly discovered lenses. The images in the middle and bottom rows are J0941+0518, OSIRIS (*left*); J2257+2349, NIRC2 (*middle*); J1640+1045, Pan-STARRS (*right*). The red stars show the source position, and the solid (dotted) lines show the caustics (critical lines) from the fits.

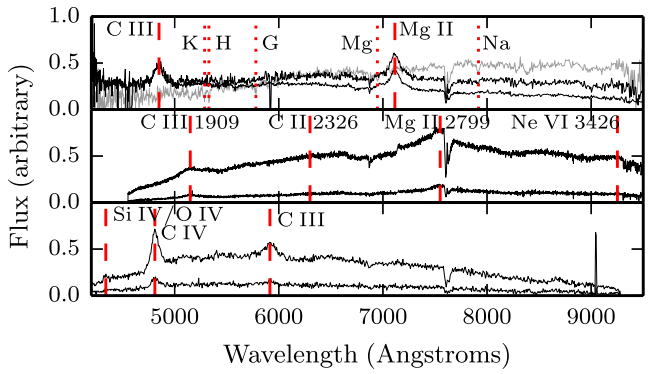

Figure 2. Spectra of the newly confirmed lenses. Emission (absorption) lines are marked with vertical dashed (dotted) lines. Note that the *A*- and *B*-band atmospheric absorption features at 7600–7630 and 6860–6890 Å should not be attributed to the quasar spectra. From top to bottom, the panels are (1) J0941+0518, ESI; (2) J1640+1045, DEIMOS; (3) J2257+2349, EFOSC2; In panel (1), the galaxy spectrum is in grey. One of the quasar spectra is contaminated by the galaxy spectrum, visible in the excess and similar features at the red end.

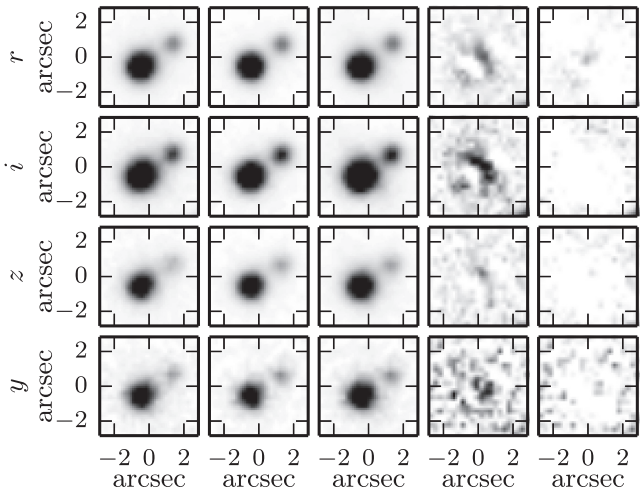

Figure 3. *Col 1*: Pan-STARRS image cutouts of SDSS J1640+1045. *Col 2*: Model 1, two point sources. *Col 3*: Model 2, two point sources plus Sérsic profile. *Col 4*: Data − Model 1; *Col 5*: Data − Model 2.

0.34 ± 0.03) arcsec (galaxy). The half-light radius of the galaxy is 1.1 ± 0.2 arcsec and the total integrated magnitudes are listed in Table 2.

2.4 SDSS J2211+1929

During the 2016 search campaigns, we blindly re-discovered the lens SDSS J2211+1929, identified by the PopMix model selection (Williams et al. 2017). This object was originally discovered as part of the Hamburg Quasar Survey as HS 2209+1914 (Hagen, Engels & Reimers 1999). This system is especially significant: due to its small image-separation, it is almost indistinguishable from a pair of point sources. Here, we show NIRC2 images obtained during the 2016 campaign on 2016 September 21. The same setup was used as for SDSS J2257+2349, but with three sets of three 120 s exposures and two additional 60 s acquisition exposures. Despite the complex point spread function (PSF) structure, an excess between the quasar images can be seen which we associate with the lens galaxy (Fig. 4, left). A simple pairwise PSF subtraction, in which Image A is subtracted from Image B and vice versa, reveals the lens galaxy as well as an Einstein ring (Fig. 4, right). These results show the importance of high-resolution imaging to securely identify lenses

Table 2. Inferred magnitudes for the two point sources and galaxy in the SDSS and Pan-STARRS cutouts of J1640+1045.

Band	PSF1	PSF2	Galaxy
SDSS-*g*	18.91 ± 0.13	20.26 ± 0.10	19.87 ± 0.30
SDSS-*r*	18.59 ± 0.08	19.94 ± 0.08	19.15 ± 0.14
SDSS-*i*	18.19 ± 0.04	19.54 ± 0.07	18.40 ± 0.08
SDSS-*z*	18.17 ± 0.31	19.52 ± 0.09	17.78 ± 0.09
Pan-STARRS-*r*	18.39 ± 0.00	19.91 ± 0.01	19.09 ± 0.03
Pan-STARRS-*i*	17.97 ± 0.01	19.47 ± 0.03	18.89 ± 0.03
Pan-STARRS-*z*	17.85 ± 0.02	19.35 ± 0.02	18.56 ± 0.03
Pan-STARRS-*y*	17.73 ± 0.02	19.23 ± 0.03	18.57 ± 0.05

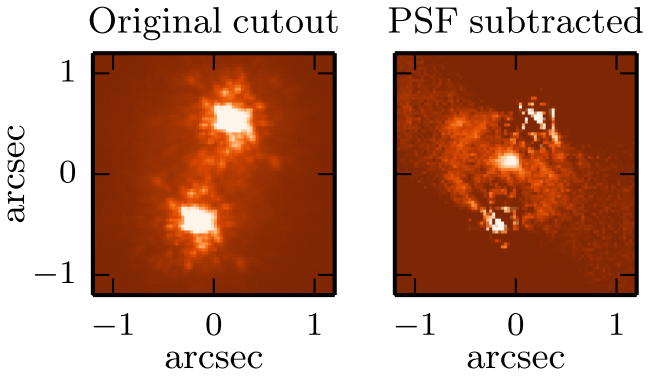

Figure 4. A PSF subtraction reveals the lens galaxy and an Einstein ring in the NIRC2 AO-assisted image of SDSS J2211+1929.

where modelling techniques such as those used for J1640+1045 are not feasible due to the small separation of the images.

3 LENS MODELS

We used the LENSMODEL package (Keeton 2011) to fit simple lens models to J0941+0518, J1640+1045, and J2257+2349. We adopt a singular isothermal ellipsoid (SIE) model, with surface density given by $\kappa = b/(2\sqrt{(1-\epsilon)x^2 + (1+\epsilon)y^2})$, where b is the lens strength, and the axial ratio q is related to ϵ by $q^2 = (1-\epsilon)/(1+\epsilon)$. Model parameters were fit using the `optimize` routine, which minimizes χ^2 by varying source and galaxy positions, source flux, lens strength b, ellipticity $e = 1 - q$, and position angle θ_e. The 1σ errors are found by determining the parameters for which $\chi^2 = \chi^2_{\rm min} + 1$. Our observational constraints are the image and galaxy positions and fluxes found using a centroid algorithm and aperture photometry for J0941+0518 and J2257+2349, and the fits from Section 2.3 for J1640+1045. We fit a model without using image fluxes and one using fluxes with 20 per cent uncertainties since flux ratios can be affected by microlensing and differential extinction (e.g. Mao & Schneider 1998; Falco et al. 1999) as well as the combined effects of quasar variability and time delays. With fluxes omitted, we have four constraints from the image positions relative to the galaxy and are fitting for b, e, θ_e, and source position. This is more free parameters than constraints and so we expect $\chi^2 \sim 0$. In this case, the fitted parameters give an idea of the correct values for the SIE model, but the errors do not hold as much meaning as those for the fits including the flux ratios.

The SIE fit to SDSS J0941+0518 infers a lens with $b = 2.88^{+0.01}_{-0.66}$ arcsec, $e = 0.37^{+0.01}_{-0.21}$, and $\theta_e = -28^{+70}_{-1}$ deg. (measured E of N) with $\chi^2 = 5.37 \times 10^{-2}$. Critical lines and caustics are plotted on the images in Fig. 1 with the inferred source position. Including a flux ratio of $1.41 \times (1 \pm 0.2)$ increased χ^2 to 30.3, but the parameter constraints improved: $b = 2.88^{+0.01}_{-0.01}$ arcsec, $e = 0.37^{+0.01}_{-0.01}$, $\theta_e = -28.2^{+0.9}_{-0.9}$ deg. The lens is in close proximity (<0.5 arcsec) to eight other sources in SDSS imaging. McConnachie et al. (2009) identify six of these objects, including the lens, as belonging to a compact group of galaxies. The additional contribution to the lens potential from the group could explain the large image separation and indicates the need for a more complex lens model.

For SDSS J1640+1045, we find $b = 0.81^{+0.40}_{-0.01}$ arcsec, $e = 0.16^{+0.09}_{-0.36}$, and $\theta_e = 0.6^{+0.1}_{-1.0}$ deg., with $\chi^2 = 8.79 \times 10^{-5}$. Including image flux ratios gives $b = 0.89^{+0.04}_{-0.04}$ arcsec, $e = 0.20^{+0.03}_{-0.03}$, and $\theta_e = 0.55^{+0.04}_{-0.04}$ deg., with $\chi^2 = 7.93 \times 10^{-5}$. This is a typical size of previously discovered quasar lenses in SDSS.

The model fit to SDSS J2257+2349 gives $b = 0.79^{+0.09}_{-0.03}$ arcsec, $e = 0.28^{+0.08}_{-0.18}$, and $\theta_e = -34^{+2}$ deg., with $\chi^2 = 2.0 \times 10^{-4}$. Here, the model only places an upper bound on the position angle. Constraining the flux ratio to be 3.85 ± 20 per cent results in a model with $b = 0.761^{+0.001}_{-0.001}$ arcsec, $e = 0.357^{+0.002}_{-0.003}$, and $\theta_e = -31.7^{+0.01}_{-0.01}$ deg., with $\chi^2 = 33.6$. These values agree with the orientation of the lens galaxy as seen in the right-hand panels of Fig. 1 and the mass centroid from the fit matches the light centroid from the images.

4 DISCUSSION AND CONCLUSIONS

We followed up 56 lensed quasar candidates selected by two photometry-based techniques, independently applied to the SDSS-DR12 data set, confirming three new lenses. AO-assisted images of J0941+0518 and J2257+2349 reveal two quasar images on either side of a lensing source, separated by 5.46 and 1.67 arcsec, respectively. Spectra confirm each system is a lens with $z_s = 1.54$ and 2.11, respectively, and $z_l = 0.343$ for J0941+0518. SDSS J1640+1045 has two quasar spectra at $z_s = 1.70$ with similar features, and the presence of the lens galaxy is secured by fits to multiband SDSS and Pan-STARRS images, where it is detected with high significance. We fit SIE models to the lenses and recover Einstein radii that are similar those of lenses in SDSS found in previous searches. With deeper data, one could apply more complex models, e.g. including external shear terms or deviations from the SIE density law, in order to better constrain the shape of the lens.

Most 'inconclusive' objects appear as two point sources in images, but do not show signs of a lens galaxy. These will require spectra to confirm if they are images of the same quasar, or, similar to the case of J2211+1929 (HS2209), deeper imaging with careful PSF subtraction. In future follow-up campaigns, a quick PSF subtraction can be used as a tool for quickly examining targets while at the telescope.

A non-negligible subset of candidates were revealed as single point sources in follow-up imaging. Their uncertain SDSS morphology was given by CCD 'blooming', which is common for bright sources and visible on some known lenses. Subsequent Pan-

STARRS images, not available at the time of this campaign, were clearer at distinguishing between spurious candidates and systems with truly multiple images.

The discovery of these lenses demonstrates the importance of photometry-based selection techniques to complement previous lens searches. None of the lenses shown here, except J0941+0518, have spectra in SDSS and thus were not explored by previous searches. The case of J0941+0518 is surprising: despite having, coincidentally, a fibre spectrum of the bright quasar image and one of the lens galaxy and counter-image, it was missed by previous spectroscopic searches. With the aim of generating a more complete sample of lenses, photometry-based searches will play an important role in exploiting the potential of new and upcoming surveys without readily available spectroscopic data.

ACKNOWLEDGEMENTS

TT acknowledges support by the Packard Foundation through a Packard Research Fellowship and by the National Science Foundation through grant AST-1450141. TA and YA acknowledge support by proyecto FONDECYT 11130630 and by the Ministry for the Economy, Development, and Tourism's Programa Inicativa Científica Milenio through grant IC 12009, awarded to The Millennium Institute of Astrophysics (MAS). CDF acknowledges support from the NSF via AST-1312329. VM acknowledges support from Centro de Astrofísica de Valparaíso. KR is supported by PhD fellowship FIB-UV 2015/2016 and Becas de Doctorado Nacional CONICYT 2017.

The authors would like to thank Cameron Lemon for useful comments and suggestions.

The acknowledgements for the telescopes and surveys used in this paper can be found at http://www.ctio.noao.edu/soar/content/acknowledgment-soar-data-publications, http://www.sdss3.org/collaboration/boiler-plate.php, https://panstarrs.stsci.edu/, and https://www2.keck.hawaii.edu/observing/keck_authors.html.

REFERENCES

Agnello A., 2017, MNRAS, 471, 2013
Agnello A. et al., 2015, MNRAS, 454, 1260
Anguita T., Schmidt R. W., Turner E. L., Wambsganss J., Webster R. L., Loomis K. A., Long D., McMillan R., 2008, A&A, 480, 327
Astropy Collaboration, 2013, A&A, 558, A33
Bonvin V., Tewes M., Courbin F., Kuntzer T., Sluse D., Meylan G., 2016, A&A, 585, A88
Braibant L., Hutsemékers D., Sluse D., Anguita T., García-Vergara C. J., 2014, A&A, 565, L11
Braibant L., Hutsemékers D., Sluse D., Anguita T., 2016, A&A, 592, A23
Browne I. W. A. et al., 2003, MNRAS, 341, 13
Buzzoni B. et al., 1984, The Messenger, 38, 9
Chambers K. C. et al., 2016, preprint (arXiv:1612.05560)
Dalal N., Kochanek C. S., 2002, ApJ, 572, 25
Dawson K. S. et al., 2013, AJ, 145, 10
de Jong J. T. A., Verdoes Kleijn G. A., Kuijken K. H., Valentijn E. A., 2013, Exp. Astron., 35, 25
Diehl H. T. et al., 2014, in Peck A.B., Benn C.R., Seamen R.L., Proc. SPIE Conf. Ser. Vol. 9149, Observatory Operations: Strategies, Processes, and Systems V. SPIE, Bellingham, p. 91490V
Ding X. et al., 2017, MNRAS, 465, 4634
Eigenbrod A., Courbin F., Meylan G., Agol E., Anguita T., Schmidt R. W., Wambsganss J., 2008, A&A, 490, 933
Faber S. M. et al., 2003, in Iye M., Moorwood A. F. M., eds, Proc. SPIE Conf. Ser. Vol. 4841, Instrument Design and Performance for Optical/Infrared Ground-based Telescopes. SPIE, Bellingham, p. 1657
Falco E. E. et al., 1999, ApJ, 523, 617
Hagen H.-J., Engels D., Reimers D., 1999, A&AS, 134, 483
Inada N. et al., 2012, AJ, 143, 119
Keeton C. R., 2011, Astrophysics Source Code Library, record ascl:1102.003
King L. J., Browne I. W. A., Marlow D. R., Patnaik A. R., Wilkinson P. N., 1999, MNRAS, 307, 225
Kochanek C. S., 2004, ApJ, 605, 58
Larkin J. et al., 2006, Mclean I.S., Iye M., in , Proc. SPIE Conf. Ser. Vol. 6269, Ground-based and Airborne Instrumentation for Astronomy. SPIE, Bellingham, p. 62691A,
Lin H. et al., 2017, ApJ, 838, L15
Mao S., Schneider P., 1998, MNRAS, 295, 587
McConnachie A. W., Patton D. R., Ellison S. L., Simard L., 2009, MNRAS, 395, 255
McMahon R. G., Banerji M., Gonzalez E., Koposov S. E., Bejar V. J., Lodieu N., Rebolo R. , VHS Collaboration, 2013, The Messenger, 154, 35
More A. et al., 2016, MNRAS, 456, 1595
Motta V., Mediavilla E., Rojas K., Falco E. E., Jiménez-Vicente J., Muñoz J. A., 2017, ApJ, 835, 132
Myers S. T. et al., 2003, MNRAS, 341, 1
Nierenberg A. M., Treu T., Wright S. A., Fassnacht C. D., Auger M. W., 2014, MNRAS, 442, 2434
Oguri M., Marshall P. J., 2010, MNRAS, 405, 2579
Oguri M. et al., 2006, AJ, 132, 999
Ostrovski F. et al., 2017, MNRAS, 465, 4325
Peng C. Y., Impey C. D., Rix H.-W., Kochanek C. S., Keeton C. R., Falco E. E., Lehár J., McLeod B. A., 2006, ApJ, 649, 616
Pindor B., Turner E. L., Lupton R. H., Brinkmann J., 2003, AJ, 125, 2325
Refsdal S., 1964, MNRAS, 128, 307
Schechter P. L. et al., 1997, ApJ, 475, L85
Sheinis A. I., Bolte M., Epps H. W., Kibrick R. I., Miller J. S., Radovan M. V., Bigelow B. C., Sutin B. M., 2002, PASP, 114, 851
Suyu S. H. et al., 2014, ApJ, 788, L35
Tewes M., Courbin F., Meylan G., 2013, A&A, 553, A120
Treu T., Ellis R. S., 2015, Contemp. Phys., 56, 17
Treu T., Marshall P. J., 2016, A&AR, 24, 11
Vegetti S., Lagattuta D. J., McKean J. P., Auger M. W., Fassnacht C. D., Koopmans L. V. E., 2012, Nature, 481, 341
Wambsganss J., 2006, Ann. Phys., Lpz., 518, 43
Williams P., Agnello A., Treu T., 2017, MNRAS, 466, 3088
Wright E. L. et al., 2010, AJ, 140, 1868
York D. G. et al., 2000, AJ, 120, 1579

SUPPORTING INFORMATION

Supplementary data are available at *MNRASL* online.

Observed_table_full.csv

Please note: Oxford University Press is not responsible for the content or functionality of any supporting materials supplied by the authors. Any queries (other than missing material) should be directed to the corresponding author for the article.

This paper has been typeset from a TEX/LATEX file prepared by the author.